



Spatial Interactions among Localized Corrosion Sites

Experiments and Modeling

T. T. Lunt,^a J. R. Scully,^{b,*} V. Brusamarello,^a A. S. Mikhailov,^c
and J. L. Hudson^{a,*}

^aDepartment of Chemical Engineering and ^bDepartment of Materials Science and Engineering,
University of Virginia, Charlottesville, Virginia 22904-4741, USA

^cFritz-Haber-Institut, Berlin, Germany

Interactions among local pit sites were investigated using a 5×5 array of 25 electrodes consisting of closely spaced, flush-mounted 316 stainless steel wires. Three types of interactions occurred when actively corroding pits existed while the remaining electrodes were initially passive in 0.05 M NaCl solution. Suppression of pitting on nearby electrodes occurred due to ohmic potential drop near pre-existing pits. Enhancement of pitting at initially passive electrodes was observed and attributed to both temporary alternations in the local solution composition and a more persistent effect attributed to some action of the locally altered solution composition on nearby passive surfaces. The exact origin of the damage on the nearby passive surface is unknown. Each of these effects exhibited different periods of persistency after pit deactivation. A phenomenological model was developed and used to simulate some of the features of the experimental findings. The model included stochastic pit initiation and interactions promoted by surface damage and concentration effects or inhibited by ohmic drop. The model successfully reproduced some of experimental observations and illustrated the formation of nonrandom corrosion damage patterns even on a simulated homogeneous surface.

© 2002 The Electrochemical Society. [DOI: 10.1149/1.1466858] All rights reserved.

Manuscript submitted May 6, 2001; revised manuscript received November 11, 2001. Available electronically March 29, 2002.

Pitting has often been assumed to be a phenomenon with events that occur randomly in time and space.^{1,2} However, previous events can have an influence on the probability of future nearby events.³⁻⁶ The spatio-temporal patterns in the concentration and potential fields during pitting are not completely understood and are difficult to predict. When a pit begins to form and current flows, the local environment is altered. Concentration changes in solution occur when metal cations enter solution and hydrolyze, bringing about an increase in both the local chloride concentration and local acidity. The environment in this way becomes more aggressive. Harb and Alkire demonstrated that the concentration gradients in solution are altered up to three pit diameters away from an active pit site.⁷ The presence of a pit site can also alter the nearby oxide film⁸⁻¹⁰ and dissolve or alter nearby sulfide inclusions¹¹ that can subsequently affect the likelihood of formation of new pits at nearby sites. Furthermore, a significant change in the potential field can occur due to the pit current.^{3,12,13} Indeed, the ohmic potential drop in solution has been measured near a pit site and found to be 75-100 mV.^{13,14} These environmental changes due to an active pit are shown schematically in Fig. 1.

The purpose here is to examine and to try to quantify the interaction among pit sites due to these three effects in a Fe-Cr-Ni alloy containing MnS and other inclusions. The increase in aggressive species concentration and damage to the oxide-covered surface adjacent to pits are both expected to increase the probability of nearby pitting. Both oxide film properties and MnS inclusion dissolution can be affected by chloride ions and acidity.^{11,15-18} In contrast, the ohmic potential drop will decrease the interfacial potential over some distance from the first pit and thereby decrease stable pit generation rates which are often strongly potential dependent.^{19,20} We wish to determine how long each effect persists, the relative strength of each, and the distances from the sustained initial pit site that are affected. Such experiments are augmented with modeling studies aimed at examining these various interactions.

Recent experimental and modeling studies have shown a dependence of current spikes associated with metastable pitting events on prior events on 316 stainless steel.^{4,6} Metastable pitting data at low (10^{-3} M) Cl^- solution concentrations approached a Poissonian, or random, distribution of the event times while at higher concentra-

tions (1 M) of Cl^- the metastable pitting events no longer occurred randomly spaced in time; the events tended to couple together as bursts of events. Autocorrelation analyses of the current-time data supported this finding by demonstrating a stronger self-correlation of the current-time data record at higher concentrations. In the present study we expand upon that temporal investigation by both exploring interactions between pit sites through the use of electrode arrays that enable examination of the spatial component of interactions and by beginning to develop a spatiotemporal model.

Experimental

Experiments were performed on arrays containing 25 electrodes arranged in a 5×5 square configuration of 0.25 mm diam 316 stainless steel wires (composition given in Table I). The arrays were made of electrode wires arranged lengthwise in a notch of a glass rod that was then filled with epoxy, as shown in Fig. 2. Specially coated wires were used which had a thin (0.009 mm) polyester coating to help prevent crevice attack along the circumference of the wires. The electrodes were electrically isolated with this type of coating and could be placed very close together, approximately 0.09 mm apart on average.

The electrode array was prepared by grinding wire cross sections flush-mounted in epoxy to a 1200 grit finish followed by 1 μm alumina polish. The array was then rinsed with deionized water. The electrode array was placed in a 3,000 wppm (0.05 M) sodium chloride solution (pH 6) along with a remotely located saturated calomel reference electrode (SCE) and a platinum wire mesh counter electrode. This cell was placed in a raised temperature water bath and experiments carried out under quiescent conditions at 47°C. Higher

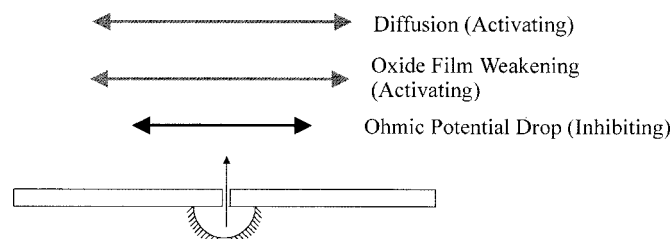


Figure 1. Schematic of the local changes that occur near a pit site. Included are changes in the local solution chemistry by diffusion, oxide film damage, and ohmic potential drop in solution.

* Electrochemical Society Active Member.

^z E-mail: jrs8d@virginia.edu

Table I. Composition of 0.25 mm diam 316 stainless steel wire (wt %).

Cr %	Mn %	Ni %	C %	Mo %	Co %	Cu %	Si %	S %	Fe
18.26	1.76	12.13	0.07	2.43	0.30	0.37	0.36	0.016	Balance

temperature than ambient was selected so that pitting would be promoted and dominant over transpassivity as the source of current increases with elevated potential. Raising the temperature enabled the use of low halide concentrations. Low chloride concentrations in test solutions made it possible that local alterations in the chemical composition near primary pits could significantly affect formation of nearby pits. Pitting studies took place on the flush-mounted cross sections of the wires exposed to solution (Fig. 2) in a downward configuration. The electrochemical conditions were controlled using a potentiostat (EG&G PAR model 273 or Pine bipotentiostat model AFRDE 4). Each electrode in the array was linked to a zero resistance ammeter (ZRA), which allowed simultaneous collection of the current from each channel over time (a second ZRA box was used when the bipotentiostat was employed to enable current collection from both sets of wires when polarized at two applied potentials). Data were collected at 20 Hz with a low pass filter (cutoff frequency of 10 Hz) using a Pentium PC with data acquisition board (Keithley DAS-1800HC2).

Potentiodynamic experiments on electrode arrays with an active or deactivated pit.—Initially all 25 electrodes in the array were scanned simultaneously using a potentiostat from -300 mV to 1.0 V SCE at a rate of 1 mV/s to establish baseline pitting potentials (*i.e.*, in absence of interactions).^d The current for each channel was recorded with the data acquisition system configured to a current range of ± 44 μ A and a resolution of 21 nA.^e Pitting potentials were taken as the potential at the remote SCE vs. the array when the current from a ZRA channel for a given electrode surpassed 30 μ A as shown in Fig. 3. Initially pitting potentials were characterized in experiments in which no pre-existing active pit was present.

Data from three types of potential sweep experiments conducted on the 25 electrode array were obtained. (Additional details can be found in Ref 3.) Experiments were performed under potentiodynamic conditions in the presence of active or just deactivated pits. In the first type of experiment a more positive potential was applied to one selected electrode in the array to activate and grow pits until they coalesced to form a large single pit across the entire electrode diameter. In these experiments a bipotentiostat was used to apply an upward potential scan on the remaining electrodes in the array. In the next experiment a bipotentiostat was used to apply a more positive potential to the left-most row of electrodes in the 5×5 array to study the effects of altered oxide covered surfaces, concentration, and potential fields created by the row of active pits. In these experiments the other 20 electrodes were scanned from 0 to 1.0 V SCE at 1 mV/s while the left row of active electrodes were driven to corrode at 1.0 V SCE (see the schematic inset in Fig. 4). The inhibiting ohmic potential drop effect was removed in a third type of experiment; in this case 1.0 V SCE was applied to the left row of electrodes for 10 min and then turned off. When turned off, the pit

^d Secondary interactions were minor near 30 μ A current, because initial pit diameters in upward scans were a small fraction of the wire electrode diameter (*e.g.*, micrometer diameter pits on a 250 μ m diameter wire). Therefore, using the fact that pit interactions were found to extend about six pit diameters away, secondary interactions would be limited to short distances for these newly formed pits that do not affect other wires in the array. This was substantiated by potential field modeling since 30 μ A currents produced negligible IR drop on other wires. In contrast, wires that were forced to pit by being driven at $+1$ V SCE developed pits across the entire wire diameter and the resulting emitted currents were much greater. These larger pits produced interactions that extended across many wires.

^e Zero resistance ammeters allowed greater currents to pass but were limited to recording the maximum setting on the range.

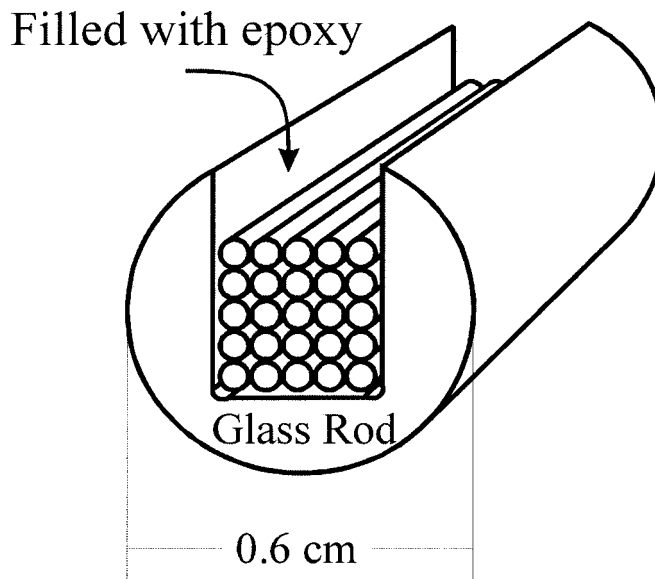


Figure 2. Schematic of the 5×5 electrode array configuration with 0.09 mm spacing. The electrode wires were positioned as close together as possible within a notch of a glass rod, then covered with epoxy.

bottom potentials drop to an open circuit potential below the pitting repassivation potential. The other 20 electrodes were either immediately scanned from 200 mV to 1.0 V SCE at 1 mV/s, in a time period of only 800 s before the concentrated solution could become diluted, or scanned after 10 min had elapsed to achieve dilution. The starting point for these scans was 200 mV SCE so that an applied potential equal to the median pitting potential could be achieved in a shorter time period. Cumulative probabilities were calculated from replicate experiments so that each cumulative probability curve involved hundreds of data points.

Potentiostatic experiments on electrode arrays with an active or deactivated pit.—Eight types of potentiostatic experiments were conducted in addition to the potentiodynamic experiments. To achieve a high resolution for the metastable pitting events that were

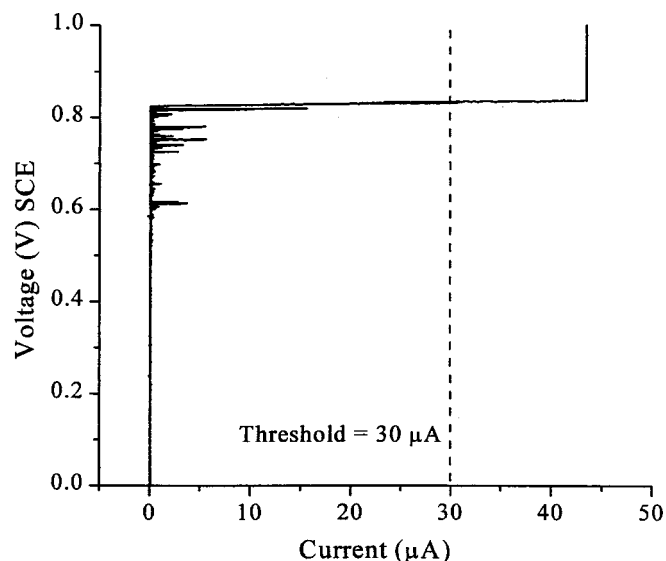


Figure 3. Potentiodynamic scan from one of the electrodes in the array when the central electrode was being driven at $+1$ V SCE. The pitting potential was taken as the remotely sensed applied potential associated with an anodic current of 30 μ A as shown.

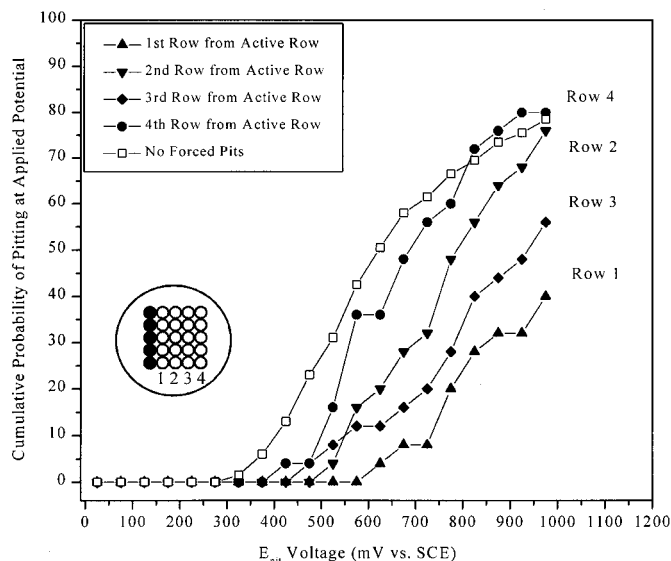


Figure 4. Cumulative pitting probabilities for remotely sensed applied potentials when all electrodes in row no. 0 are held at 1 V vs. SCE to create stable pit sites. The effect of the active pit sites can be seen to strongly decrease the cumulative probability of pitting on row no. 1 and die off by row no. 4 (where the probabilities are close to the unpitted base line experiments).

present in the current signal, the data acquisition system was reconfigured to a range of $\pm 2.8 \mu\text{A}$ with a resolution of 1.35 nA. The smallest events that were resolved were approximately 20 nA in size while most of the metastable events were not larger than the 2.8 μA maximum. The base case (with no driven electrodes) was established by using a single potentiostat to hold all 25 electrodes at the same potential, either 200, 250, or 300 mV SCE, while the current signal was collected at 20 Hz.

The driven electrode experiments were performed with the central electrode held at 1.0 V SCE while the remaining 24 electrodes were simultaneously held at constant potentials of either 100, 200, 300, 400, or 500 mV SCE in separate experiments. The potential field effect was removed (leaving the solution concentration and oxide film effects) by using a single potentiostat to drive the central electrode at 1.0 V for 10 min and then removing this applied potential while a constant potential was maintained on the remaining 24 electrodes. Potentials of 200, 250, and 300 mV SCE were applied for these concentration experiments. Experiments with a bipotentiostat were similarly conducted by driving an entire row of electrodes at 1.0 V SCE while the remaining 20 electrodes were held at a second potential (200, 300, 400, and 500 mV).

Similar deactivated pit experiments were performed with an entire row of deactivated pits. One row of five electrodes was held at 1 V vs. SCE for 10 min and then returned to open circuit before applying a potential of either -50, 0, 50, 100, or 150 mV vs. SCE to the remaining 20 electrodes. The deactivated-row experiments were repeated, but with a 10 min delay added after turning off the applied potential of the prepitted row of five electrodes. This allowed time for the concentration and oxide film effects to dissipate so that the persistence of these effects could be determined. Finally, the oxide film effect was further isolated by stirring the solution vigorously for 60 s after turning off the applied potential on the row of active pit sites (in order to remove completely any concentration field in solution).

Results and Discussion

Results from potentiodynamic experiments with active or deactivated pits.—An E vs. I curve for a single potentiodynamic scan is shown in Fig. 3. Replicate scans produced on freshly pol-

ished electrodes were used to calculate the cumulative probabilities of achieving stable pitting during such potentiokinetic scans at each remotely sensed applied potential.^f Figure 4 shows the results of the cumulative pitting probabilities calculated by row for experiments in which the probabilities were calculated separately from data for wires in each row of electrodes when the left most row was actively pitting. The row of active pits emitting high current was row no. 0. Row no. 1 was closest to these active electrodes while row no. 4 was furthest away. The baseline case in which all 25 of the electrodes were scanned simultaneously (with no driven active or deactivated pit electrodes) is also shown to facilitate comparison such that any deviation caused by the presence of the active row of pit sites can be detected. As can be seen from Fig. 4, all four rows of electrodes experienced cumulative probabilities for stable pitting that were lower at each potential applied during upward scans than in the case when there were no pre-existing active pits. These results indicate that the ohmic potential drop associated with the left row of active pits was dominant in these experiments. Furthermore, a pronounced difference was present between the electrodes in the row closest to the actively corroding electrodes compared to those that were furthest away. The closest row, row no. 1, was found to have only pitted during potentiodynamic scans at significantly higher remotely sensed applied potentials than the ones that were farther away. When compared to the no-pitting base case, a 300-350 mV more positive applied potential was required to reach the same probability of pitting. The row furthest away, row no. 4, was nearly unaffected by the active row of electrodes and experienced pitting at applied potentials near that of the base case. The large difference in behavior between the closest row (row no. 1) and the most distant row (row no. 4) demonstrates the extent of ohmic potential drop which exists near the active row (row no. 0). This effect disappears at the most distant locations suggesting minimal alteration in the potential field due to current being emitted from the active first row.

Similar experiments were conducted in the case of a just-deactivated row of electrodes. An entirely different trend was seen, however, when upward scans were conducted on remaining electrodes. Cumulative pitting probabilities, again calculated according to distance from the prepitted electrodes, demonstrate the effect of proximity to the pit sites (with row no. 1 closest to the recently deactivated row and row no. 4 furthest away) as shown in Fig. 5. Sites closest to the deactivated row, (e.g., row no. 1) demonstrated significantly higher cumulative probabilities for stable pitting at each applied potential during upward scans compared to the unpitted baseline experiments involving upward scans of all electrodes without prepitting. The remaining three rows of electrodes show a more limited deviation from the baseline case with cumulative pitting probability curves that often cross.

These two sets of experimental results are significant in that they show the large effect that active or recently deactivated pits can have on the probabilities of stable pitting associated with the surrounding electrode area. Figure 6 compares the pitting probabilities of row no. 1 (the closest row) from the two experiment types: the solid triangles are from the experiments with a concurrent active-row of pits and the open triangles are from experiments involving the just-deactivated row. The locally altered chemical environment and/or surface oxide film or inclusion alterations caused by proximity to the just-deactivated row of pits was nearly as strong in increasing pitting probabilities at row no. 1 as the ohmic potential drop was in suppressing pitting when an adjacent row of stable pits was active. For instance, none of the row no. 1 electrodes in the active-row experiments had experienced a stable pit at the same applied potential of 500 mV, while over 65% had undergone stable pit formation in the just-deactivated pit row experiments.

^f Statistical distributions in potentials associated with stable pitting are often attributed to distributions in pit induction times^{19,20} and variable distributions from electrode to electrode in the fatal surface flaw that serves as the site of stable pit. This particularly occurs on electrodes of small diameter approaching the MnS inclusion spacing.

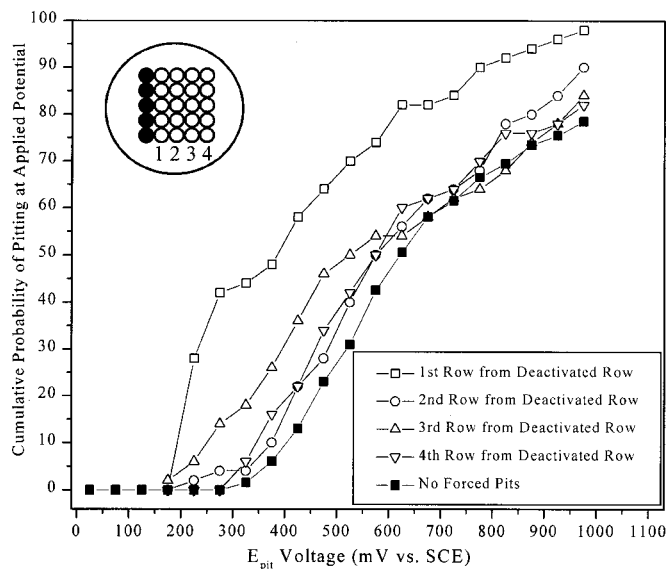


Figure 5. Cumulative pitting probabilities when all electrodes in row no. 0 were held at 1 V vs. SCE for 10 min and then returned to OCP to create deactivated pit sites. The effect of the just-deactivated pit sites can be seen to most strongly alter the pitting probabilities on row no. 1.

Results from potentiostatic experiments with an active or deactivated pit.—Stable pitting induction times, collected during potentiostatic experiments on the 25 electrode array, were also analyzed to determine what effect, if any, concurrently driven or the prior driven electrode(s) that underwent stable pitting had on the stable pit induction times of the remaining electrodes. Induction times for the remainder of the electrodes in the array were defined by the time at which the current exceeded 2.8 μA for significant time periods (see Fig. 7).

Figure 8 depicts the state of the electrodes at various times for one experiment from five different potentiostatic experiments. Electrodes in gray are those on which a stable pit has naturally formed while electrodes in black are those on which pits were formed across

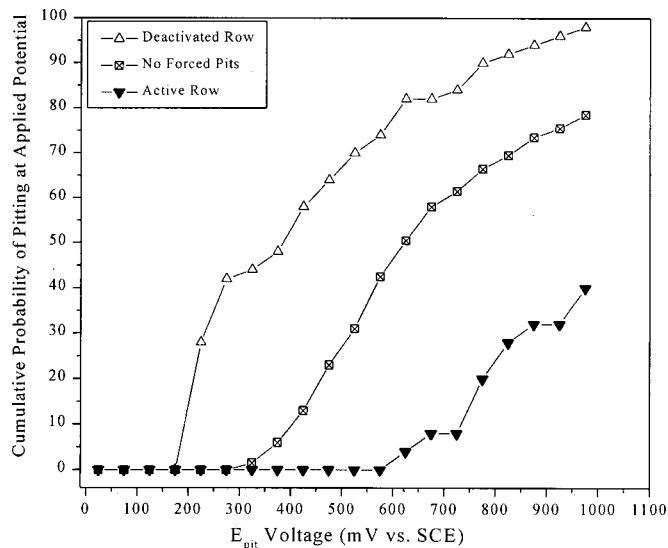


Figure 6. Cumulative pitting probabilities demonstrating the large change in pitting probabilities caused by the active (solid triangle) or deactivated (open triangle) row of electrodes on the closest row (row no. 1). The probabilities for baseline experiments in which no large active rows were present at the start of upward scans are included for reference.

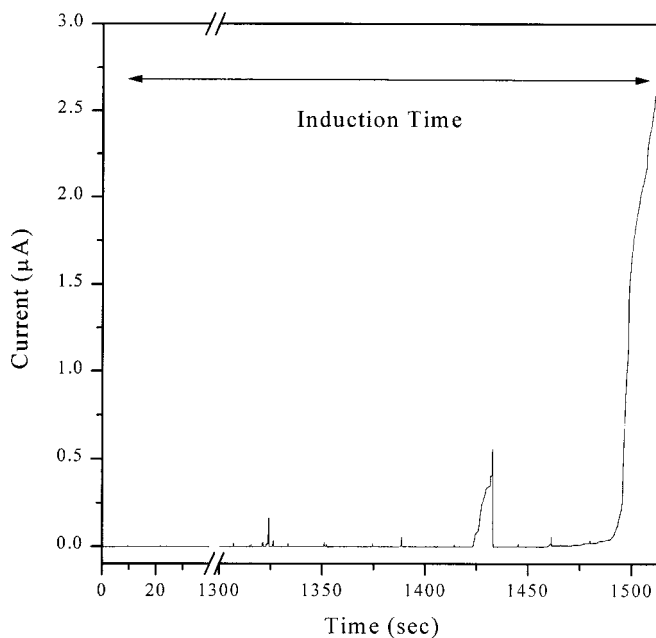


Figure 7. Current-time series collected during potentiostatic experiments when the central electrode was held at 1 V vs. SCE while 300 mV vs. SCE was simultaneously applied to the remaining 24 electrodes.

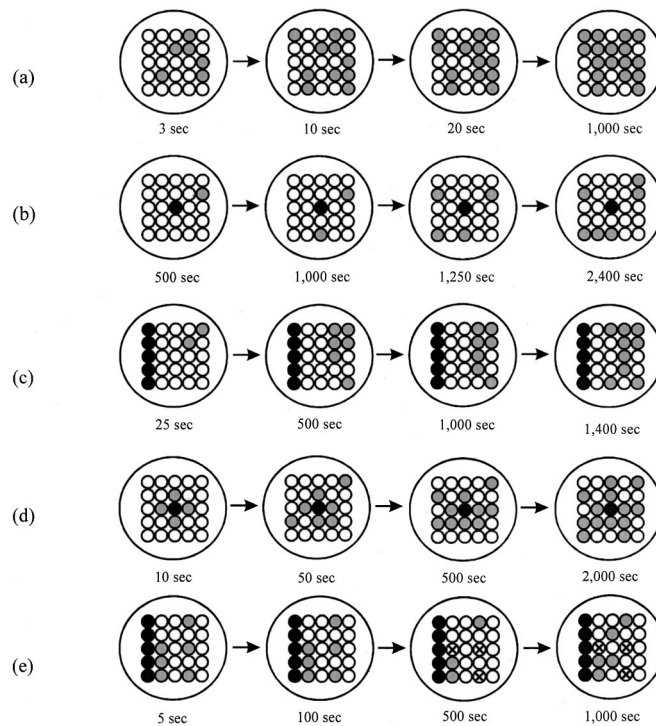


Figure 8. Sites of stable pit formation at various times during potentiostatic experiments in which black indicates an electrode which was active or deactivated (driven at 1 V vs. SCE) and electrodes in gray have formed a stable pit by the time indicated: (a) no active or deactivated electrodes were used (300 mV), (b) center electrode was active (300 mV), (c) row of electrodes was active (500 mV), (d) center electrode was deactivated (300 mV), and (e) row of electrodes were deactivated (0 mV). The Xs indicate electrodes on which a stable pit formed but later repassivated during the experiment.

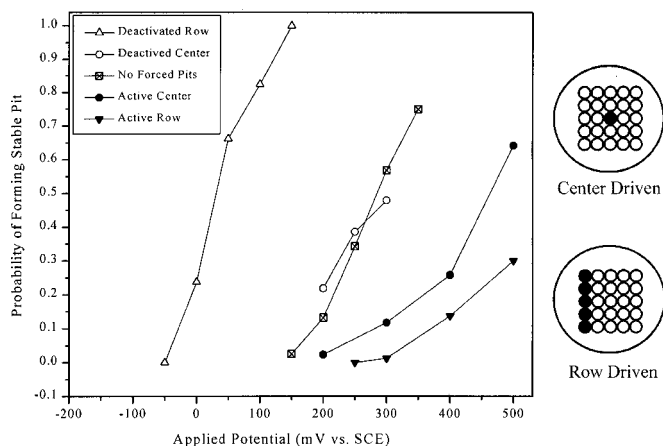


Figure 9. The cumulative probability of forming a stable pit at each applied potential for five types of potentiostatic experiments based on the percentage of electrodes on which a stable pit has formed by 1,000 s.

the entire wire diameter when driven using the bipotentiostat. Figure 8a shows the result when no forced (active or deactivated simulated pit sites) were present and all electrodes were held at 300 mV vs. SCE. No apparent pattern in the formation of stable pit sites can be seen.⁸ In the second potentiostatic experiment, shown in Fig. 8b, the central electrode was held at 1 V vs. SCE while the remaining 24 electrodes were simultaneously held at 300 mV vs. SCE with the bipotentiostat. New pit sites still formed on other electrodes but only further away from the active central electrode. The effects due to active pitting sites were amplified by holding an entire row of electrodes at 1 V vs. SCE while the remaining 20 electrodes were held at 500 mV as shown in Fig. 8c. Again, new pits tended to form only further away from the active row of electrodes and higher potentials were required to cause pitting to occur. In fact, no electrodes closest to the active row ever demonstrated a pit in any experiment up to 500 mV vs. SCE.

The potential field effect was removed (leaving only the concentration and oxide film/inclusion effects) by using deactivated stable pit sites (*e.g.*, sites which have been allowed to corrode for a period of time to form a pit across the entire wire but then stopped prior to applying a potential to the remaining electrodes). In Fig. 8d, the remaining 24 electrodes were held at 300 mV vs. SCE after the pit at the central electrode was deactivated. In this experiment, electrodes closest to the deactivated central electrode exhibited a stable pit after shorter induction times compared to pits that formed on electrodes that were farther away. Similarly, in Fig. 8e, one row of electrodes was held at 1 V vs. SCE for 10 min and then returned to open-circuit potential before applying a potential of 0 mV vs. SCE to the remaining 20 electrodes. Figure 8e shows that pits would occur closest to the deactivated site, but not on electrodes in the fourth row distant in the time period of the experiment. Also note the low potential, only 0 V vs. SCE, which could cause pitting to occur in these deactivated-row experiments. When 0 V vs. SCE was applied to an electrode array in which no large forced pits (active or deactivated) were present, 0 V vs. SCE would not be high enough to cause any pitting to occur at any location on the array in these time periods.

While a visual examination of the schematic drawings in Fig. 8 is helpful in assessing relative pitting susceptibility, it would be advantageous to obtain more quantitative results. Numeric values for pitting susceptibility from potentiostatic experiments were calculated by determining whether a stable pit had formed on an electrode during a 1,000 s period. The percentage of pitted electrodes can then be easily found from the collection of current data for each remotely sensed applied potential. The results from the five main types of

experiments are presented in Fig. 9. These experiments included potentiostatic tests with no actively driven pits, active center and active row of pits, as well as deactivated center and deactivated rows of pits. Stable pits were formed in the baseline case with no pre-existing active driven pits at potentials between 150 to 350 mV. Stable pitting probabilities, defined by induction within 1000 s, ranged from 3 to 75%. Lower applied potentials, near 150 mV, resulted in no metastable or stable pitting. In comparison, higher potentials near 350 mV, caused almost instantaneous pitting of all electrodes. The behavior seen in experiments with just-deactivated central electrode pits was similar to the case of no active pits. There was little influence from the deactivated site. However, when an entire row of electrodes had been prepitted at 1 V vs. SCE for 10 min just prior to applying potentials to the 20 other electrodes, the potentials required to produce a high probability of pitting shifted to lower applied potentials by 200 to 250 mV. Applied potentials, such as 50-100 mV vs. SCE, which could not have caused a stable pit to initiate in the baseline experiments (*e.g.*, with no pre-existing active pit as large as a wire diameter), resulted in almost certain stable pit formation when one row of electrodes had been prepitted for 10 min. Significant shifts in pitting probabilities were also found with both types of active electrode (center and row) experiments. In contrast, applied potentials between 200 and 500 mV vs. SCE were required with a central active electrode to produce pitting probabilities of 2 and 64%, respectively. Nearly the same range of potentials, 250 to 500 mV, yielded far lower pitting probabilities of 0 to 30% when an entire row was actively pitting (Fig. 6). Comparing the results with an active central pit to the unpitted case, the remaining electrodes in the active-pit experiment behaved as if they were actually experiencing interfacial potentials which were 50-150 mV lower than the remotely applied potential. Therefore, it became quite difficult to force stable pitting to occur on neighboring electrodes when simultaneously active pit sites were present. In contrast, it became very easy when a row of prepitted sites was just deactivated; this effect can be accounted for by either changes in local solution concentration or by an increase in surface damage.

The same qualitative trends were observed when metastable pitting was examined on electrodes adjacent to and far from an actively pitting row. When all rows adjacent to an actively pitting row were held at +400 and 500 mV vs. SCE, metastable pitting was suppressed on wires adjacent to the actively pitting row. Metastable pitting was enhanced on wires in row 4 during active pitting at row 1.

Isolation of concentration from oxide/inclusion damage effects.—To try to discover the time period over which the concentration and oxide film/inclusion damage effects endured, variations in the deactivated time and solution stirring were investigated. However, since the oxide film/inclusion properties can change with time at open-circuit potential (OCP), the effect of exposure time at OCP on the pitting probabilities in the absence of any other interactions was first examined to eliminate this variable. The maximum time delay for these control experiments was judged to be 25 min (equal to a 5 min hold period before applying any potential to any electrode + a 10 min period of active pitting of the left row + a 10 min delay period). Therefore, the baseline (no pre-existing active pits) experiments were repeated by first allowing the array to remain at OCP in solution for 25 min followed by applying the potential of interest. Figure 10 shows that at most applied potentials there was no change in the probability of stable pit formation. A slightly lower pit probability (deviation of 9%) was found at 350 mV, which was considered insignificant. The key result was that resting at OCP did not alter the pitting probability of the array. Thus, any changes seen in the longer-exposure experiments must be due to the effects of solution chemistry changes induced by the deactivated electrodes and not from natural oxide film changes due to exposure time in the bulk solution at OCP.

Once these baseline data had been established, the effect of a delay after deactivating a row of pits was examined. After prepitting

⁸ Again, this confirms lack of significant secondary interactions for the length scales of these wire arrays.

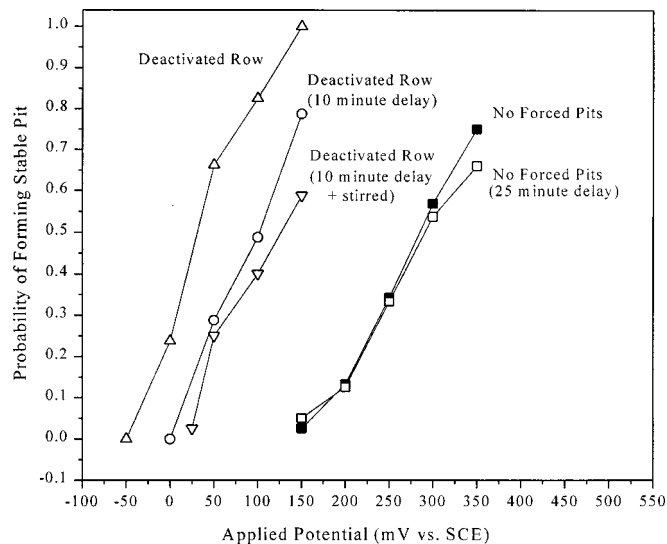


Figure 10. The cumulative probability of forming a stable pit at each applied potential for three time-delayed potentiostatic experiments (and the two nondelayed experiments for comparison) based on the percentage of electrodes on which a stable pit has formed by 1,000 s.

the left row of five electrodes for 10 min at 1 V vs. SCE, the potential was removed and all 25 electrodes remained at OCP for another 10 min. The chosen potential was then applied to the 20 unpitted electrodes and their current monitored. Figure 10 shows that the pitting probabilities at each potential were higher than in the baseline case but lower than in the nondelayed, just-deactivated row case. At 0 mV the pitting probability dropped from 24 to 0% and at 150 mV it dropped from nearly 100 to 79%. Therefore, in that 10 min period of time either (or both) the aggressive species concentrated near the pitted row diffused into the bulk solution or the surface was able to repair to a sufficient degree to partially recover the baseline pitting properties of the electrodes in the array. However, there were still significant increases in the stable pitting probability as compared to the unpitted experiments implying that a significant amount of residual surface damage was still present despite ample time for species transport and mixing in the electrolyte and possible surface aging and healing. Even after 10 min, interactive effects had endured and were present which made the array persist in being much more susceptible to stable pitting.

In the final experiments, the concentrated aggressive species near active pits was removed (leaving only the surface oxide film or inclusion damage) by vigorously stirring the cell's solution for 60 s after pit deactivation followed by a 10 min rest at OCP. Pitting probabilities calculated using data from these experiments are also shown in Fig. 10. Surprisingly, a considerable increase in the pitting probabilities (compared to the unpitted baseline experiments) is still present even after removing any remnants of a solution-phase concentration gradient. It is clear that these effects persist or endure for longer times than ohmic potential effects that vanish upon removal of applied current to active pits.

Spatial variation of the result from the just-deactivated row potentiostatic experiments are considered in Fig. 11 where the stable pitting probabilities are calculated based on distance from the deactivated row of pits. A dramatic shift above the baseline case persists at all locations, but there is a smaller difference in pitting probabilities among the various locations. For instance, row no. 4 is almost as affected by the row of deactivated pits as row no. 1, and all locations are exhibiting strong tendencies to pit well below the minimum required applied potential in the baseline case for upward scans (which was 150 mV vs. SCE). Only small differences between rows were found in these experiments. At each potential the pitting probabilities vary only by as much as 10-15% between the closest and

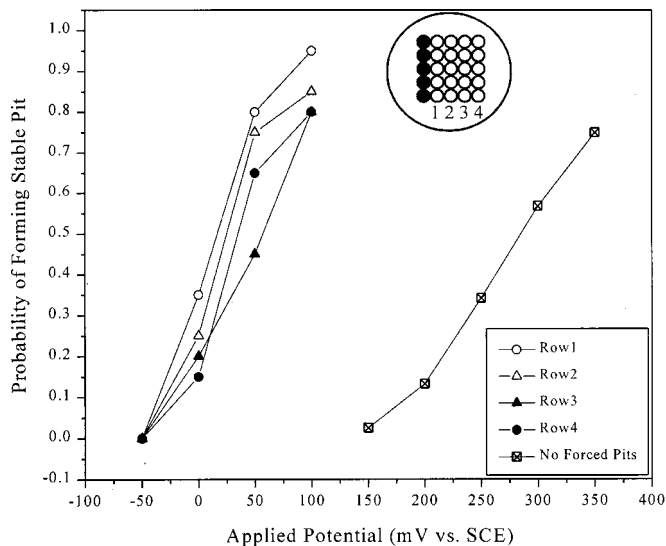


Figure 11. The cumulative probability of forming a stable pit at each applied potential for the deactivated-row-of-pits experiments based on distance from the deactivated sites. The cumulative probabilities were calculated using the percentage of electrodes on which a stable pit has formed by 1,000 s.

most distant row of electrodes. The last two rows, no. 3 and no. 4, have similar pitting probabilities such that their curves cross twice. Note that the results of Fig. 11 are significantly different from the case where an active row of pits was present (Fig. 4). In comparison it is clear that the distance over which the ohmic potential drop dominates interactions differs from the distance over which concentration field or surface damage effects operate.

One of the most significant findings from the experiments discussed above is the persistent surface damage effect. This was disclosed by stirring experiments after an active row of pits was deactivated when nearby electrodes exhibited persistent reduced resistance to stable pit formation. One possibility is that surface damage occurs to nearby inclusions to provide sites for pit formation. Consider the following scenario. The active pits increase the local $[\text{Cl}^-]$ and $[\text{H}^+]$ concentrations in the vicinity of this pit site. Both oxide film properties and MnS inclusion dissolution on neighboring surfaces can be affected by highly concentrated chloride ions and acidity, but many studies on stainless steels indicate that pits almost always form at inclusions.²¹ Ti-free stainless steels containing Mn exhibit a variety of sulfide inclusions including the possibility of Fe, Cr, Mn, as well as Ca sulfides.²² Eklund showed that MnS inclusions dissolve chemically at a more rapid rate below about pH 4.8 releasing H_2S .¹⁶ Baroux has shown that sulfide-containing stainless steels exhibit lower pitting potentials in acidic solutions due to sulfide damage.²³ Studies by various groups suggest that sulfur-rich inclusions form H_2S by chemical dissolution at low potentials and thiosulfate by electrochemical processes at high potentials.^{24,25} MnS dissolution is also catalyzed by presence of Cl^- .²⁶ Both sulfide and thiosulfate species can be detrimental to the pit resistance of stainless steel.²⁷ In this study, one speculation is that both acidification and raised Cl^- concentration associated with primary pits could damage sulfur-rich inclusions on nearby electrodes rendering these surfaces more susceptible to pitting.

Model: Development, Simulation, and Discussion

We now describe a model where the effects of both metastable and stable pitting on the pitting initiation susceptibility of the surfaces adjacent to the primary pits are examined. In this model the pitting events are initiated as functions of both time and position. The long-term goal of such a model is to simulate and interpret the

trends seen in experiments. The model presented here is one step in that development and is guided by the observations made above.

In an earlier study we developed a stochastic model of the temporal behavior of localized corrosion (see Ref. 4 for details). A feature of the model is that each pitting event can influence subsequent events, although the influence of an individual event decays with time. The memory effect is substantiated by the experimental results shown above. Chiefly, ohmic shielding which can reduce the interfacial potential by hundreds of millivolts inhibits both stable and metastable events. Such high ohmic potentials were established (Fig. 7 in Ref. 3) and shown to extend over the entire 5×5 electrode array when an active row pitted at 0.7 A/cm^2 . In addition, either concentration effects or oxide/inclusion damage can promote pitting on adjacent surfaces.

In the present paper we modify the model in two ways. First, we include spatial effects, that is, we investigate the interactions among pit events at different locations; a one-dimensional electrode geometry is chosen for simplicity although this shall be extended to two dimensions in later studies. Second, we begin to develop the dependency of the memory on physical phenomena, viz., the potential drop, concentration, and surface damage in the vicinity of the stable and metastable pits. These parameters were selected because they clearly exert influence as shown in the above experiments. In the model initial metastable pits form stochastically or stable pits are designated for certain locations. All subsequent pit events are governed by a pit generation rate that is affected by a memory term that is hindered by potential drop and enhanced by both local Cl^- concentration and surface damage. These effects were shown to be operative in experiments above. Thus, we consider a combination of stochastic (initiation) and deterministic (memory) effects in the pit pattern formation mechanism under conditions mimicking potentiostatic control as discussed above.

The memory is taken to be dependent on three environmental parameters, each of which depends on position as well as time and each of which changes as a result of the metastable or active pits formed at earlier times. The three factors are concentration, ohmic potential drop, and the damage of the surface (passive film or sulfide inclusions) on the electrode surface under an assumed fixed applied potential. Thus, the memory term is taken to be composed of three effects

$$M_n = \alpha_C C_n + \alpha_F F_n - \alpha_\phi \phi_n \quad [1]$$

where M_n is the memory at location n , C_n is the concentration of aggressive species, F_n is the extent of the film damage, ϕ_n is the ohmic potential drop in solution, and the three values of α are proportionality constants. This memory is then used to calculate the new probability of forming a pit at each location in the array, w_n

$$w_n = \frac{w_0}{1 + \exp\left(\frac{M_0 - M_n}{H}\right)} \quad [2]$$

where M_0 and H are scaling factors that affect how strongly the memory will influence the generation of new events and w_0 is the maximum possible generation rate. Hence, the present model considers enhanced or reduced metastable pit initiation rates based on the above three factors.

All three of the interaction mechanisms are results of the flow of current from the electrode once pitting occurs. The total anodic current describes the rate of production of the metal cations that bring about changes in the local solution concentration (e.g., acidification and Cl^- transport). Additionally, the current produces the ohmic potential drop in solution. As in the previous version of the model,⁴ the current for newly initiated events is characterized in the model by a sharp rise followed by an exponential decay. (Both exponential decay and rise can be seen in experiments, depending on the metal and conditions.) In the present model, the exponential decay in current was assumed. However the current is not limited spatially to the

initiation site of the event: pits grow. Therefore, the current (j_n) is a function of both time and distance from the initial site of activation

$$j_n = j_0 \exp\left[-\frac{(\Delta x)^2}{2d(\Delta t + \varepsilon)} - \frac{\Delta t}{\tau}\right] \quad [3]$$

where $\Delta t = t - t_k$ and $\Delta x = x - x_k$.

The k th event is initiated at time t_k , at position x_k . The current at site n is a function of the distance from the initial pit site, where this distance is denoted as Δx . The squared dependence on Δx gives a reasonable decay of current with position. The current has maximum value of j_0 and a decay time of τ . The parameter d governs the rate of spreading of the current. The quantity ε is added to prevent division by zero initially; it is a small quantity and does not affect the subsequent calculated values.

The concentration of aggressive species at a location along the array is calculated from the current (which produces more of the species), diffusive transport along the surface of the array, and transport away from the surface of the electrode into the bulk solution (by either migration or diffusion). Thus, the change in concentration at any location can be expressed as

$$\frac{\partial C_n}{\partial t} = \gamma(C_{\text{bulk}} - C_n) + D\left(\frac{C_{n-1} - 2C_n + C_{n+1}}{\Delta x^2}\right) + \beta \cdot \sum_k j(\Delta t, \Delta x) \quad [4]$$

The value of D selected for initial simulations was $10^{-5} \text{ cm}^2/\text{s}$. However, it could be varied to account for stirring effects or convective mixing. In initial calculations of solution transport by diffusive processes from an active electrode of the dimensions of our wires, the concentration field decayed to ambient levels at a distance of about one electrode length after 10 s, but reached a steady-state concentration profile at a distance of about five electrode lengths after about 600 s and was unchanged from this at about 1000 s. Recall that most experiments above were conducted over this time frame. These calculations support the experimental observation that concentration fields could affect every electrode in the 5×5 array after 600 s.

The ohmic potential drop in solution was calculated using Newman's solution for an active current emitting disk (in our case as pit) embedded in an insulating material with a counter electrode at infinite distance.¹² The resulting potential drop is found using Eq. 5

$$\Phi_n(\Delta t) = \Phi_n^{\text{max}} \exp\left(-\frac{\Delta t}{\theta}\right) \quad [5]$$

The maximum potential drop, Φ_n^{max} , is a function of location as described using rotational elliptic coordinates (ξ, η)

$$\Phi_n^{\text{max}} = \Phi_0 \left(1 - \left(\frac{2}{\pi}\right) \tan^{-1} \xi\right) \quad \text{with} \quad \Phi_0 = \frac{j_0}{4\kappa a} \quad [6]$$

where κ is the solution conductivity and a is the disk radius. See Newman's paper for more details.¹² As shown in Ref. 3, a substantial potential drop can be seen over a distance of 0.1 cm (several electrodes) in the dilute 0.05 M NaCl used here when 0.7 A/cm^2 current density is emitted from a pit the size of a single wire electrode. Accordingly, a smaller potential drop will be seen for smaller metastable pit currents when a pit is only a few micrometers in diameter. For these simulations, the decay time constant for the ohmic potential field was assumed to be the same as the decay time constant for the current, $\theta = \tau$.

Finally, an equation for the oxide film/inclusion damage had to be created, although the exact mechanism for the damage is unknown at present. It was assumed that the changes in the oxide film were directly related to the local increase in the aggressive species, which adsorb to or alter the film/inclusions. Therefore, a simple linear dependence of the surface change (at each location n) on the

solution concentration was used. The film could then be healed with time (e.g., reform or thicken with time in the case of an oxide), so a decay based on the time constant, Γ , was also included

$$\frac{dF_n}{dt} = C_n - \frac{1}{\Gamma} F_n \quad [7]$$

These equations were used in a one-dimensional spatial simulation on a 1 mm long electrode that was divided into 600 locations, each eligible to form a metastable pit (1.7 μm) due to interactions. The concentration equation (Eq. 4) was solved using an adaptive step size Runge-Kutta algorithm. Four different sets of conditions were used in the simulations to create situations similar to those employed experimentally. Initially, the current is zero at all locations (except in simulations where a stable pit is pre-existing). After an event occurs by random chance, the ohmic potential drop everywhere along the electrode as well as the concentration and initial film damage are calculated at all locations using the equations discussed above. From these three terms, the memory and in turn the new generation rate at each location are determined. A random number is generated and compared to the pit generation rate at that site. If the random number is smaller than the generation rate, a metastable pit is generated. A positive memory effect increases the chance of more events. Hence, the memory term causes pit generation to deviate from randomness. After all sites are considered the time is incremented, and the current is recalculated based on the initiation time and location of previous events; the process is then repeated.

Simulations in which no pre-existing driven (active or deactivated) electrodes were present were performed, and the results from one simulation are shown in the plots in Fig. 12. A total of 171 metastable pitting events occurred in 2,000 s as shown in the current plot in Fig. 12a. The individual effects produced by the space-time plots of the concentration, film and ohmic potential drop are shown in Fig. 12b, c, and d, respectively. In Fig. 12a, b, and d, the white background represents current, concentration, and ohmic voltage drop approaching zero. Black or gray indicates values of these parameters greater than zero as indicated by the scale to the right of each figure. The film damage is depicted in Fig. 12c as red areas where the blue background indicates little or no damage. The resulting total memory based on a sum of the effects as given by Eq. 1 is shown in Fig. 12e as a function of location and time. The memory in Fig. 12e ranges from orange through yellow, green, and blue for a negative (suppressing new pit generation) memory, red for no memory, while darker red-grays represent positive (promoting new pit generation) memory. Each metastable pitting event created a temporary pit current that suppresses interaction due to the negative memory associated with the associated ohmic potential drop. This negative memory dominated compared to the temporary enhancement in solution concentration. However, the ohmic interaction was a function of the instantaneous current and thus died quickly as the current flow from individual pits decayed. After the inhibitive ohmic shielding effect dissipated, the darker red-gray activating or pit promotion memory effect remained due to the more persistent solution concentration and surface damage memories. In particular, the surface damage creates a wake in time-position-memory space that persists long after the pits have died. Note that the concentration field also decays fairly rapidly from diffusive transport. Convective transport is not incorporated here but would make this process occur even more quickly. Using the appropriate memory function, it can be seen that the dominant factor in creating a positive (pit producing) memory is the surface damage effect, which endures for several thousand seconds using the inputted model parameters. This mimics the observed experimental results where damage persists even after deactivation of an active pit or row of pits as seen in Fig. 5, 6, and 9-11. The overall result was the promotion of a cascade of metastable pitting events induced by the enhanced positive memory. Figure 12f shows a histogram of the total number of metastable pit events by location after 2000 s along the electrode. The metastable

pitting events are concentrated in one location, where the memory was strongest, with only a few isolated events occurring at other locations. These isolated events died out without resulting in a cascade of events. Note that in future modeling, surface damage could be linked to the physical process occurring at the surface. For instance, there might be a limited number of sulfide-type inclusions that could be damaged in a given area or a finite number of metastable pit sites that could be depleted.

To simulate experiments in which part of the electrode array was driven at a higher voltage to create stable pitting locations, model simulations were performed in which the center 10 segments of the 1 mm wide electrode (17 μm wide pit) were preselected as the site of a stable pit. This stable pit generated a constant 1 A/cm² current density as seen by the dark band in the center of the current space-time plot in Fig. 13a. Here, the white background represents a low or near-zero current indicative of passive dissolution. Metastable pits are seen to occur at a distance of about 0.1 mm away from the stable pit in a band which widens over time. Near the stable pit, the ohmic potential drop caused the total memory to be negative which suppressed the formation of any metastable pit sites as can be seen by the space-time plot of the current shown in Fig. 13a and memory in Fig. 13b (note that blue, green, yellow, and orange again represent a negative memory and darker gray-red regions represent a positive memory). However, surface damage and/or concentration effects had a longer spatial range than the ohmic potential drop according to model parameters producing a widening zone of positive memory about 0.1 mm away from the stable pit. This promoted activation of metastable pit events in a widening zone approximately 5-10 pit diameters (85-170 μm) away from the active site, demonstrated by the metastable pits which can be seen in the current in Fig. 13a. However, each metastable pit temporarily inhibits pitting in this memory band due to the ohmic drop from its own current. At still greater distances, there was zero memory. The short (spatial) range inhibition due to the ohmic voltage field and long range enhanced susceptibility to pit generation are shown in Fig. 13c by the histogram of the location of metastable pit events. The two separate clusters of events can clearly be seen with no metastable pits near the center where the ohmic potential drop from the stable pit site prevents the nucleation of new events. Recall that this accurately simulates the situation observed experimentally in Fig. 4 and 6 where the ohmic effect dominates pitting susceptibility out to distances of four electrodes away from the active site in the five-electrode experimental array. Future experiments will confirm this effect using longer experimental arrays.

The experiment in which an electrode was temporarily driven as a stable pit for 10 min and then stopped (to create a deactivated pit site) was also simulated using this model. The central part of the electrode section (17 μm) was again assumed to corrode at 1 A/cm² for 600 s and then to be subsequently turned off. Shown in Fig. 14a and b are the current and resulting total memory, respectively. Metastable events were only allowed to form after the current from the central pit was deactivated. A total of 117 metastable pitting events occurred after the stable pit repassivated. These metastable events are clusters in the center of the electrode with some of the metastable pits even forming inside the previous pit. A very strong negative memory (indicated by blue, green, yellow in Fig. 14b) exists near the center stable pit during the first 600 s due to ohmic shielding that operates when the central pit is active. Smaller temporary regions of negative memory due to ohmic potential drop are observed only near the metastable pit sites that emit their own current after 600 s. However, a large positive memory (dark red regions in Fig. 14b) through the center of the electrode continued after the stable pit site was deactivated due to the persistent oxide/inclusion damage mechanism. In contrast, lighter red total memory regions further away from the center indicate zero memory. The overall result is similar to experimental findings of Fig. 10 and 11, where oxide/inclusion damage enhanced subsequent pit susceptibility even after stirring to remove concentration gradients. Two forks or separated regions of higher memory appear to form after the central pit

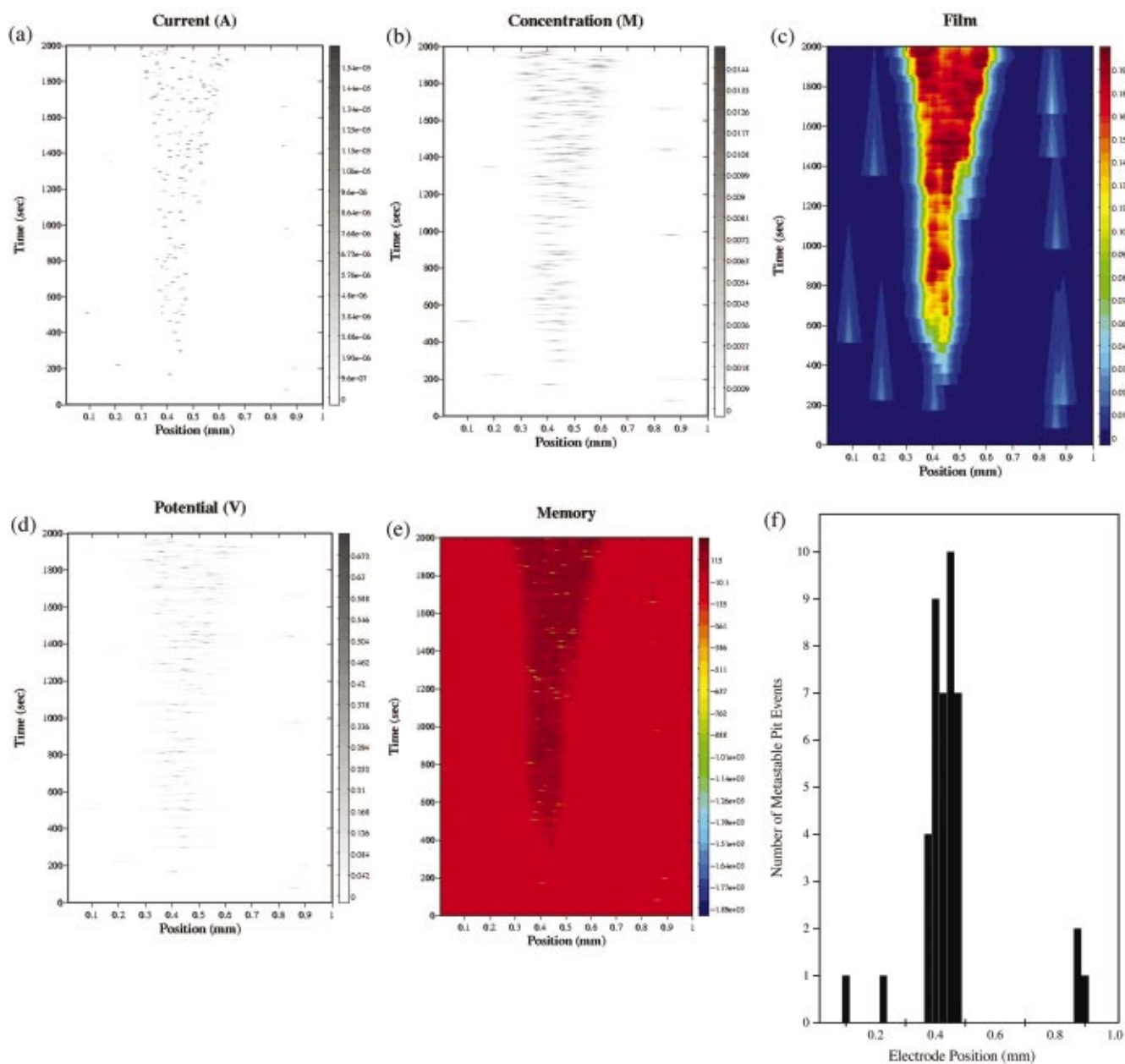


Figure 12. Simulation showing the occurrence of metastable pits along a 1 mm long electrode. (a) Space-time plot of the current with the gray scale on the right indicating current level in amperes; (b) solution concentration with a gray scale indicating locally enhanced concentration in mole per liter; (c) surface damage with blue regions indicating zero damage; (d) the potential field with the gray scale on the right indicating the ohmic voltage level in volts; (e) total memory where yellow, green, and blue indicated negative memory, red indicates no memory and gray-red indicates positive memory; (f) histogram of the number of metastable pit events which occurred across the electrode.

site is deactivated. These are due to the metastable pits which formed early in those two areas causing further activation and increased metastable pitting activity at those locations on the electrode. However, this is not a generic finding to be expected in every simulation. This bimodal behavior is shown more clearly in Fig. 14c, a histogram of the total number of metastable pit events by location along the electrode after the end of the simulation. This histogram in Fig. 14c demonstrates that the metastable pitting events occurred primarily in the center of the electrode array near the position of the previous active pit with only a few scattered events in other locations.

These spatial simulations reproduce many of the features of the experiments. When no stable pit sites are active, metastable pits activate future events resulting in an increase in metastable pitting

activity or stable pit formation. It is unlikely, however, that this type of metastable pitting behavior would continue indefinitely. Either the increase in the rate of metastable pitting and metastable pit current density would lead to the formation of a stable pit, or the events would die out as the preferential nucleation sites were consumed. Both effects have been observed experimentally.^{28,29} In future simulations, both the transition to stability and a limited number of nucleation sites can be added to the spatial model in order to more closely simulate realistic behavior. For instance, the model was configured so that a transition from metastable pitting to stable pitting occurred when the current reached a stabilization threshold. Amidst the metastable pits that formed in Fig. 15a, two sites exceeded the current threshold and transitioned into stably growing pitting sites. These two sites can be seen by the black bands in the current space-time

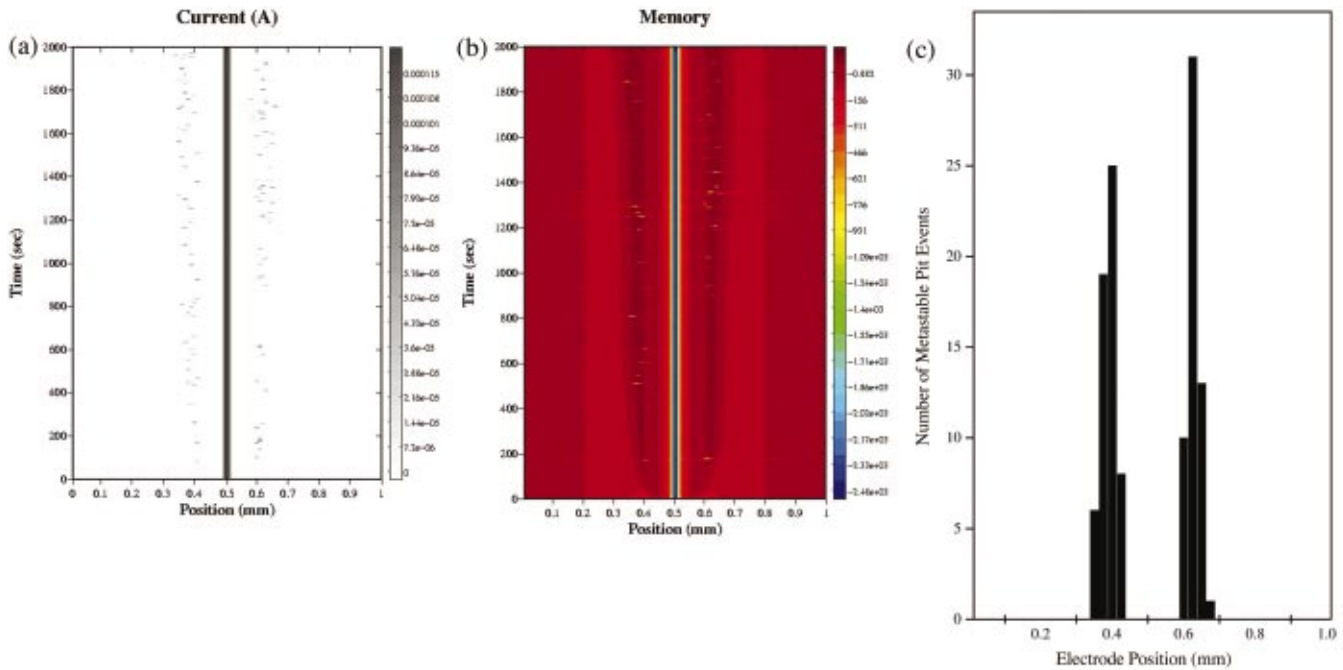


Figure 13. Simulation in which the central 17 μm of the one-dimensional electrode was driven as an active pit site. (a) Space-time plot of the current with the gray scale on the right indicating current level in amperes; (b) the total memory where yellow, green, and blue indicated negative memory, red indicates no memory, and gray-red indicates positive memory; (c) the histogram showing the number of metastable pit events that occurred across the electrode.

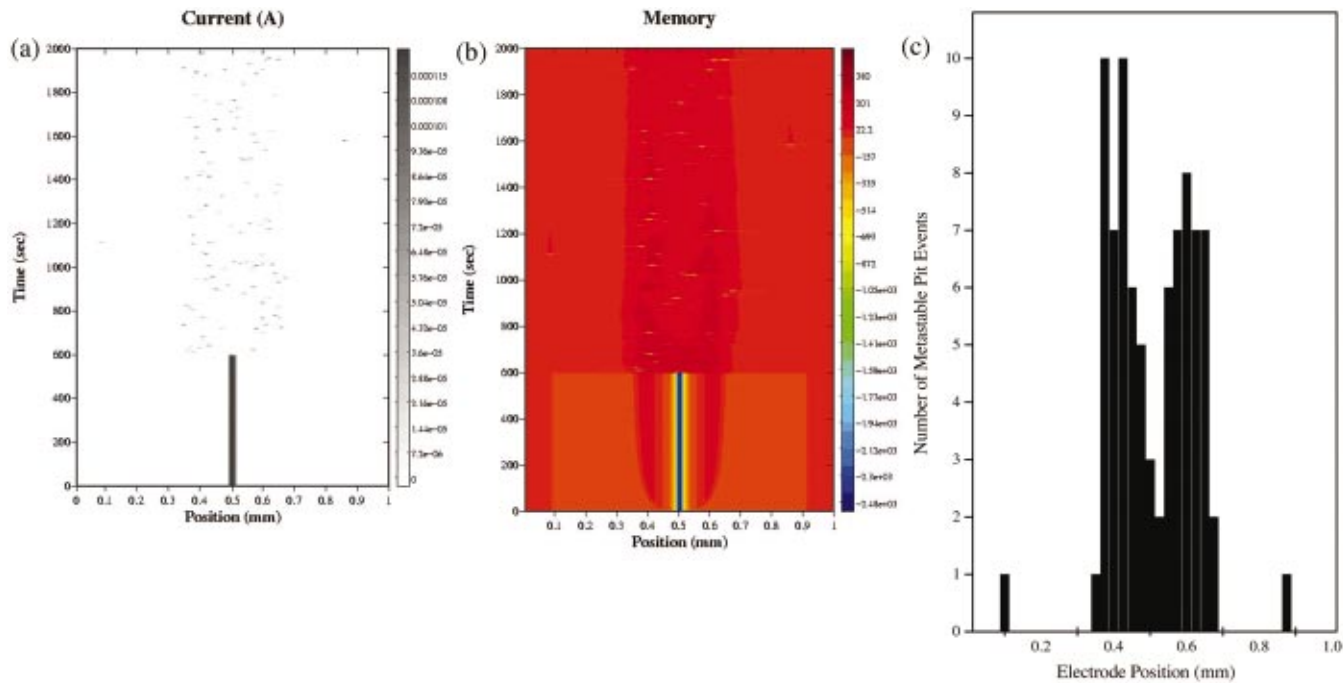


Figure 14. Simulation in which the central 17 μm of the one-dimensional electrode was driven as a stable pit for 600 s and then shut off. (a) Space-time plot of the current with the gray scale on the right indicating current level in amperes; (b) total memory where yellow, green, and blue indicated negative memory, red indicates no memory and gray-red indicates positive memory; (c) histogram showing the number of metastable pit events that occurred across the electrode.

plot in Fig. 15a. The memory that results from these two stable, as well as the metastable, events is shown in Fig. 15b. The number of events as a function of position is shown in Fig. 15c.

Conclusions

An active or deactivated pit can influence the probability of nearby future pitting events. Active or deactivated simulated pit sites

were found to produce changes in the stable pitting generation rate that strongly suggest a significant effect of the local concentration of aggressive species in solution, alterations in potential field, and damage to adjacent oxide/inclusion covered surfaces. Potential field alteration suppressed subsequent pitting while concentration effects and surface damage both enhanced future pit events. All three of these interactive effects were found to have a very strong influence

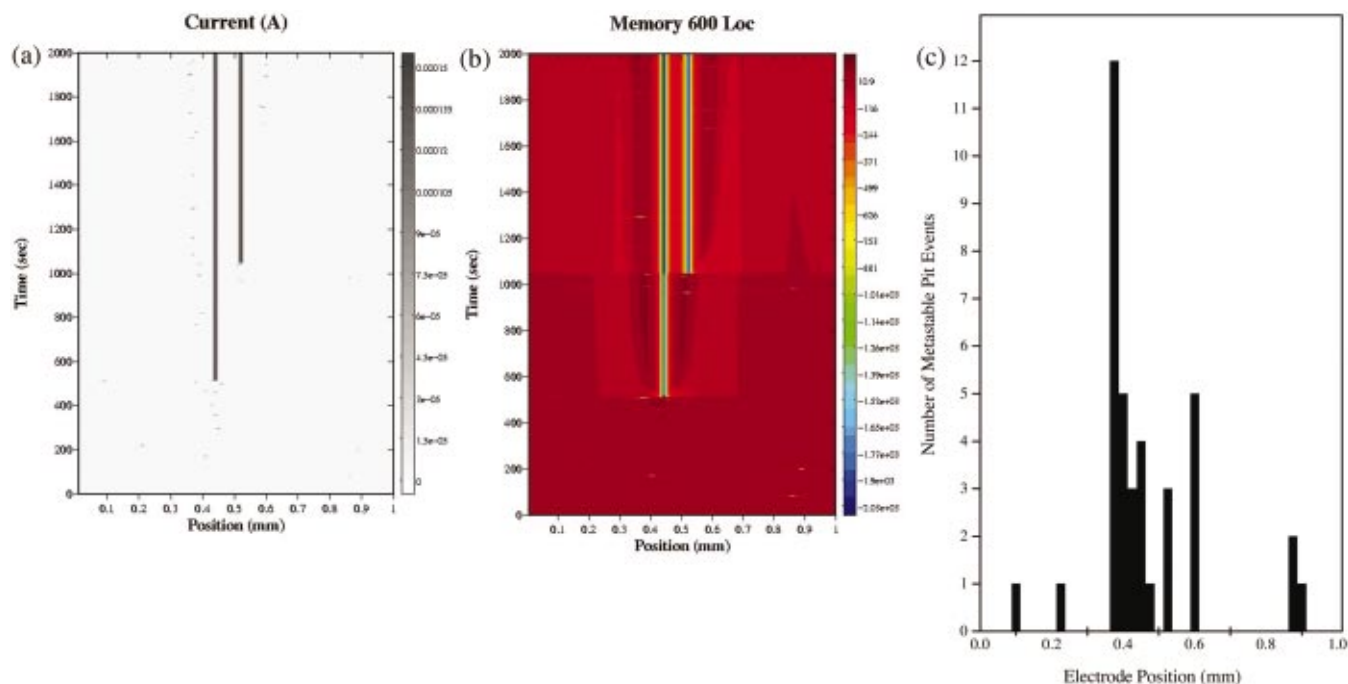


Figure 15. Simulation showing transition to a stable pit as the memory exceeds 100. (a) Space-time plot of the current with the gray scale on the right indicating current level in amperes; (b) total memory where yellow, green, and blue indicated negative memory, red indicates no memory and gray-red indicates positive memory; (c) histogram showing the number of metastable pit events that occurred across the electrode.

on the experimental pitting susceptibility up to five pit diameters away from an electrode serving as an active pit site in experiments and five to ten diameters away in model simulations. However, each influence operates on its own distance and time scales. Specifically, the surface damage effect persisted long after ohmic potential drop effects and concentration field effects decayed. Thus the formation of one stable pit lowers the resistance of the adjacent electrode surface to subsequent pitting long after the time period over which the other effects produced any interactions. A model was developed which captured these three interaction effects. It could easily be shown in the model that surface damage was the most persistent effect by increasing the memory factor associated with this interaction. The different interaction distances and memories associated with the three factors incorporated in the model produced nonrandom patterns of pit damage on a model homogeneous electrode surface.

Acknowledgments

This work was supported by the United States Department of Energy, Office of Basic Energy Sciences, Division of Materials Sciences and Engineering under contract DEFG02-00ER45825 with Dr. Yok Chen as contract monitor. The work was also supported by the National Science Foundation. Equipment and software support by Perkin Elmer Corporation and Scribner Associates, Inc., is gratefully acknowledged.

University of Virginia assisted in meeting the publication costs of this article.

References

- C. Gabrielli, F. Huet, M. Keddam, and R. Oltra, in *Advances in Localized Corrosion*, H. S. Isaacs, U. Bertocci, J. Kruger, and S. Smailowska, Editors, National Association of Corrosion Engineers, Houston, TX (1990).
- G. A. Henshall, *J. Nucl. Mater.*, **195**, 190 (1992).
- T. T. Lunt, V. Brusamarello, J. R. Scully, and J. L. Hudson, *Electrochem. Solid-State Lett.*, **3**, 271 (2000).
- B. Wu, J. R. Scully, A. S. Mikhailov, and J. L. Hudson, *J. Electrochem. Soc.*, **144**, 1614 (1997).
- U. Bertocci, M. Koike, S. Leigh, F. Qiu, and G. Young, *J. Electrochem. Soc.*, **133**, 1782 (1986).
- T. T. Lunt, S. T. Pride, J. R. Scully, A. S. Mikhailov, and J. L. Hudson, *J. Electrochem. Soc.*, **144**, 1620 (1997).
- J. N. Harb and R. C. Alkire, *J. Electrochem. Soc.*, **138**, 2594 (1991).
- K. Sugimoto, S. Matsuda, Y. Ogiwara, and K. Kitanwra, *J. Electrochem. Soc.*, **132**, 1791 (1985).
- Y. Xu, M. Wang, and H. W. Pickering, *J. Electrochem. Soc.*, **140**, 3448 (1993).
- T. P. Hoar, D. C. Mears, and G. P. Rothwell, *Corros. Sci.*, **5**, 279 (1965).
- C. S. Brossia, in *Critical Factors in Localized Corrosion III*, R. G. Kelly, G. S. Frankel, P. M. Natishan, and R. C. Newman, Editors, PV 98-17, p. 326, The Electrochemical Society Proceedings Series, Pennington, NJ (1999).
- J. Newman, *J. Electrochem. Soc.*, **113**, 501 (1966); J. Newman, D. N. Hanson, and K. Vetter, *Electrochim. Acta*, **22**, 829 (1977).
- G. Butler, H. C. Kolson, and A. D. Mercer, *Br. Corros. J., London*, **16**, 31 (1971).
- I. L. Rosenfeld and I. S. Danilov, *Corros. Sci.*, **7**, 129 (1967).
- B. MacDougall and M. J. Graham, *J. Electrochem. Soc.*, **131**, 727 (1984).
- G. S. Eklund, *J. Electrochem. Soc.*, **121**, 467 (1974).
- G. Wranglen, *Corros. Sci.*, **14**, 331 (1974).
- S. E. Lott and R. C. Alkire, *J. Electrochem. Soc.*, **136**, 973 (1989).
- T. Shibata and T. Takeyama, *Corrosion (Houston)*, **33**, 243 (1977).
- T. Shibata and H. Takamiya, in *Critical Issues in Reducing the Corrosion of Steels*, H. Leidheiser, Jr. and S. Haruyama, Editors, p. 17 NACE, Houston, TX (1985).
- P. Forchhammer and H. J. Engell, *Werkst. Korros.*, **20**, 1 (1969).
- M. Smailowska, Z. Szklarska-Smailowska, A. Szummer, and M. Rychcik, *Corros. Sci.*, **9**, 123 (1969).
- B. Baroux, in *Corrosion Mechanisms in Theory and Practice*, P. Marcus and J. Oudar, Editors, pp 265-309, Marcel Dekker, New York (1995).
- C. H. Paik, H. S. White, and R. C. Alkire, *J. Electrochem. Soc.*, **147**, 4120 (2000).
- D. E. Williams and Y. Y. Zhu, *J. Electrochem. Soc.*, **147**, 1763 (2000).
- Y. Y. Zhu and D. E. Williams, *J. Electrochem. Soc.*, **144**, L43 (1997).
- R. C. Newman, *Corros. Sci.*, **24**, 331 (1985).
- P. C. Pistorius and G. T. Burstein, *Philos. Trans. R. Soc. London, Ser. A*, **341**, 531 (1992).
- N. J. Laycock, S. P. White, J. S. Noh, P. T. Wilson, and R. C. Newman, *J. Electrochem. Soc.*, **145**, 1101 (1998).